Available online at www.sciencedirect.com
ScienceDirect
Energy Procedia 00 (2008) 000–000
Energy Procedia
www.elsevier.com/locate/XXX

GHGT-9

Characterizing fault-plume intersection probability for geologic carbon sequestration risk assessment

Preston D. Jordan[a1], Curtis M. Oldenburg[a], and Jean-Philippe Nicot[b]

[a]*Lawrence Berkeley National Laboratory, 1 Cyclotron Road MS90-1116, Berkeley, CA 94706 USA*
[b]*Bureau of Economic Geology, University of Texas at Austin, PO Box X, Austin, TX 78713 USA*

Elsevier use only: Received date here; revised date here; accepted date here

Abstract

Leakage of CO_2 out of the designated storage region via faults is a widely recognized concern for geologic carbon sequestration. The probability of such leakage can be separated into the probability of a plume encountering a fault and the probability of flow along such a fault. In the absence of deterministic fault location information, the first probability can be calculated from regional fault population statistics and modelling of the plume shape and size. In this study, fault statistical parameters were measured or estimated for WESTCARB's Phase III pilot test injection in the San Joaquin Valley, California. Combining CO_2 plume model predictions with estimated fault characteristics resulted in a 3% probability that the CO_2 plume will encounter a fault fully offsetting the 180 m (590 ft) thick seal. The probability of leakage is lower, likely much lower, as faults with this offset are probably low-permeability features in this area.

PACS: Type pacs here, separated by semicolons ;

Keywords: geologic carbon sequestation, fault leakage risk, fault encounter probability

[1] Corresponding author. Tel.: 00 1 510 486-6774; fax: 00 1 510 486-5686.
E-mail address: pdjordan@lbl.gov.

1.Introduction

The potential for leakage of CO_2 via fault zones is an area of considerable uncertainty for geological storage of CO_2 [1]. The probability of leakage can be separated into the probability of CO_2 encountering a fault and the probability of flow out of the storage region via that fault. Fault zone properties vary considerably, with some fault zones forming recognized conduits for fluid flow, as commonly evidenced by springs co-located with fault zones, and others forming barriers to fluid flow, as evidenced by many hydrocarbon reservoirs created in part by sealing faults. There is currently little consensus regarding a methodology for characterizing fault zone properties in the deep subsurface with respect to their potential as leakage pathways. In contrast, research regarding fault population statistics has reached a moderate level of consensus. While there are certainly further interesting questions and unsettled issues in this field, it is sufficiently mature to be constructively applied to risk assessment involving potential fault zone leakage of CO_2 from prospective storage reservoirs. In this study, we present a method for using fault population statistics to estimate the probability of a CO_2 plume encountering a fault, and apply this method to WESTCARB's Phase III pilot test injection at the Kimberlina power plant in the southern San Joaquin Valley, California.

2.Plume-fault encounter probability

A method for calculating the probability of a plume encountering one fault (an event *g*) given information on fault density can be derived from point counting statistics. This is represented in Figure 1 which shows 100 randomly located plumes, which are represented by circles, and a single randomly located fault of size *L*.

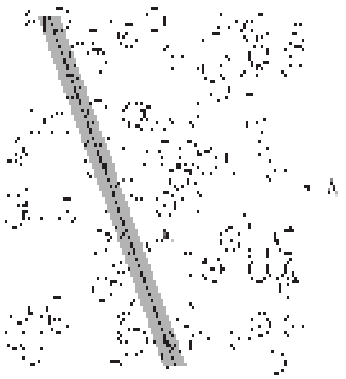

Figure 1. Diagram of 100 randomly located, circular plumes and a randomly located fault. Any plume geometrically centered within the shaded area will encounter the fault.

Figure 1 indicates that in general the probability of *g* is given by

$$\Pr(g) = A_f / A_0 \tag{1}$$

where A_0 is the total area being considered. This approach assumes that the fault or faults cross the entire area of interest, and that each plume only encounters one fault. The first condition is equivalent to assuming that faults are large relative to A_0, and the second condition is equivalent to assuming the spacing between faults is large relative to the plume diameter. As the spacing between large faults is generally greater than between small faults, these assumptions are qualitatively in agreement.

With these assumptions, if a plume is centered within a distance equal to the plume radius, *r*, of a fault, *g* will occur. Given that the fault has two sides

$$A_f = 2rL \tag{2}$$

where L is the length of fault in the study area (shown on Figure 1). L can also be written as the areal fault density F times A_o:

$$L = FA_0 \quad (3).$$

Substituting Equation 3 into 2, 2 into 1, and canceling terms gives

$$\Pr(g) = 2rF \quad (4).$$

The value of F must be measured from fault maps, and the value of r can be approximated by numerical simulation. If the plume margin is some shape other than circular, then Equation 4 can be generalized to any plume shape by substituting half the plume dimension perpendicular to the fault, s:

$$\Pr(g) = 2sF \quad (5).$$

The value of s can be measured directly from plots of the area swept by mobile CO_2 as modeled by numerical simulation.

3.Fault density

Field studies, physical modeling, and numerical simulations [2, 3, 4] have indicated that the relationship between the density of faults greater than a certain size (length or displacement) versus that size is often power law. starts exponential at low strains, rapidly transitions to power law as strain increases, stays power law as strain increases further, becomes exponential again at high strains and finally becomes “characteristic” at very high strains with one or few faults dominating as shown on Figure 2 [4, 5]. Figure 2 shows that the slope of the fault density distribution increases with increasing strain. The negative of this slope is C_d, which consequently declines with increasing strain. At initiation of strain, many small faults develop, and so C_d is large. As strain continues, some of the faults grow and eventually link, while few new small faults develop, so C_d decreases. At very high strains, further development of one fault tends to dominate, and the fault population evolves toward a “characteristic” fault population, akin to a characteristic earthquake population.

The power law formulation of fault density is

$$F \propto d^{-C_d} \quad (6),$$

where d is the displacement cutoff (the size above which all faults are included to calculate a particular density). Taking the log of Equation 6 gives

$$\log F \propto -C_d \log d \quad (7).$$

For power-law fault populations, substituting Equation 6 into Equation 5 with the addition of a proportionality constant B gives

$$\Pr(g) = 2sBd^{-C_d} \quad (8).$$

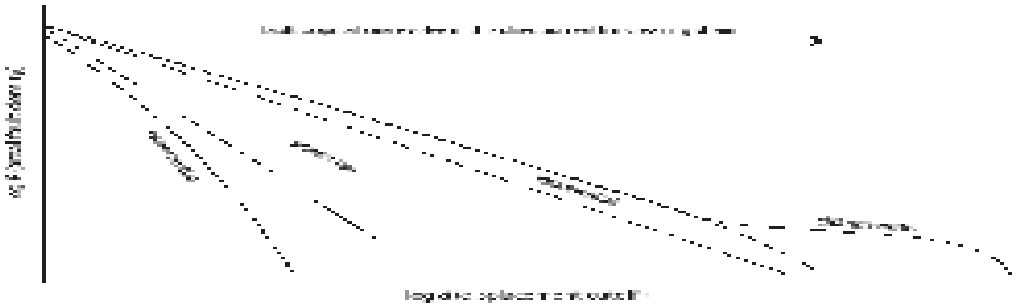

Figure 2. Typical evolution of fault populations [4, 5].

4.Case study: WESTCARB's Kimberlina Phase III Pilot Test

WESTCARB's phase III pilot test will consist of the injection of 250,000 metric tonnes (275,500 tons) per year of CO_2 for four years at Clean Energy System's Kimberlina power plant located northwest of Bakersfield in California's San Joaquin Valley. The CO_2 will be injected into the Vedder Formation at a depth of approximately 2,200 meters (7,200 feet). The lower Miocene Vedder Formation consists of interlayered marine sandstones and shales averaging 160 m (520 ft) in total thickness in the vicinity of the site. The sandstones generally comprise 50% of the formation thickness.

The Vedder Formation is overlain by the lower Miocene Freeman-Jewett Formation. This 180 m (590 ft) thick unit is a marine shale and siltstone with thin sandstone beds. It is regionally extensive and is believed to provide a continuous seal over the Vedder Formation.

4.1.CO_2 plume simulation

The injection was numerically simulated using the ECO2 equation of state package of TOUGH2 [6, 7]. This code incorporates hysteretic formulation for capillary pressure and relative permeability [8], allows for salt precipitation and dissolution, but does not account for fluid-rock chemical reactions. While the code can account for non-isothermal conditions, for computational efficiency during this study a constant reservoir temperature was imposed.

Figure 3 shows a plan view of the simulated three-dimensional plume. Note that injection into each sandstone in the Vedder was simulated, which results in a stack of plumes. The area shown is only for the uppermost sandstone.

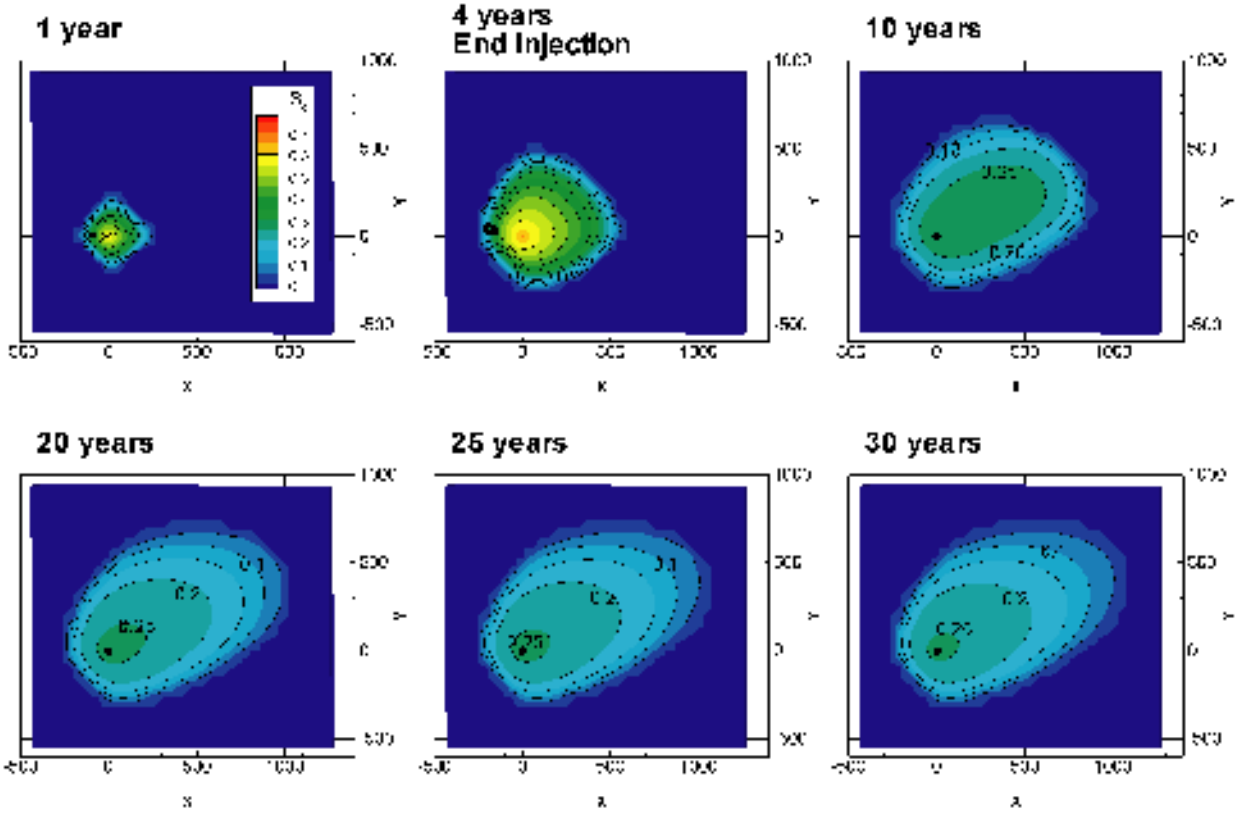

Figure 3. Extent of numerically simulated supercritical phase CO_2 from the Kimberlina injection. North is up. (Simulation result courtesy of Christine Doughty, LBNL, via personal communication.)

4.2.Fault density

The position and displacements of faults in the vicinity of the Kimberlina site are not currently available. However, there are numerous oil and gas fields within a 25 km (15 mi) radius of the site. The position of these fields relative to the Kimberlina site is shown on Figure 4.

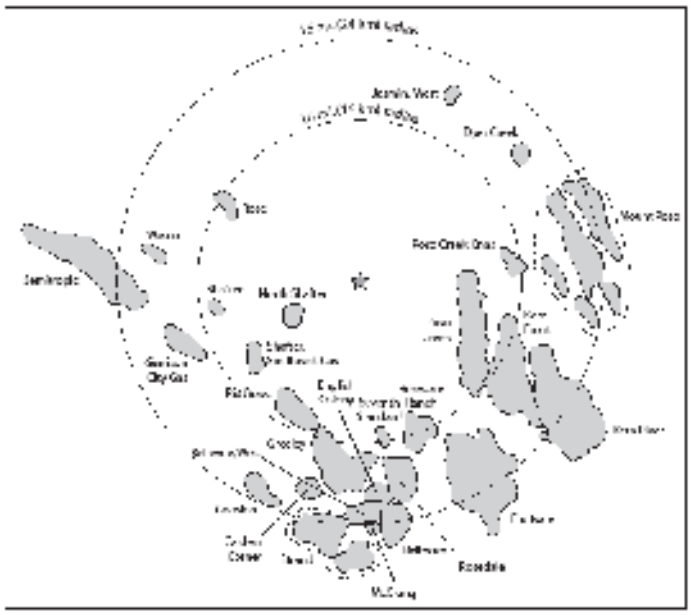

Figure 4. Oil and gas fields in the vicinity of the Kimberlina site (located at the star). North is up. [9]

Structure maps are available for each of the oil fields shown in Figure 4 [9]. Map area, and fault lengths, throws, and orientations were measured from these maps. While the maps are variously based on different horizons, analysis of the resulting data indicates that the fault density is relatively constant across the stratigraphic section covered by these maps, which includes the Vedder. Analysis indicates the fault density is somewhat higher to the northeast of the Kimberlina site than to the southwest, positioning the site at a location of likely average fault density for the data set. Fault orientations show a shift from a bimodal fault orientation at greater distance from the Kimberlina site, to a monomodal, almost north-south orientation closer to the site.

Using the measured areas, and fault lengths and throws, log-log plots were constructed of fault density versus throw truncation (Figure 5). Throw truncation is the logical equivalent to displacement cutoff for throw (vertical offset). As most of the faults in the vicinity of Kimberlina are subvertical, using throw truncation instead of displacement cutoff does not introduce significant error. While it is tempting to see the fault density distribution as exponential given the good fit to the data, we note that low displacement faults are always underreported due to the fault mapping resolution limit [9]. As a result, the actual fault population is always larger than the measured data at the low end of the range. The exponential fit, as good as it is, actually underpredicts the fault density at low throw truncations.

The throw truncation interval and range of values fitted were varied to find the largest range that could be fit linearly. This resulted in a line that lies above the data at low throw cutoff, in accord with the mapping resolution effect. The point of departure of the linear fit from the fault-density data is at a throw cutoff of approximately 65 ft (20 m). This is reasonable as it is slightly lower than the most common contour interval of 100 ft (30 m) for the oil and gas field structure maps. Consequently, the linear fit appears more likely to represent the actual fault population in the vicinity of the Kimberlina site, indicating that the fault population follows a power-law distribution. The power law fit also yields higher fault density estimates, which makes it more conservative than the exponential fit for estimating leakage risk.

a) b)

Figure 5. Fault density versus throw truncation: a) all data with exponential fit and selected data with linear fit, and b) selected raw data (open squares) with linear fit (lighter weight line) and selected data corrected for the "finite-range effect" [9] with linear fit (heavier weight line).

The linear fit also over predicts the fault density at high throw truncations relative to the data according to Figure 5a. This occurs due to the probability of under sampling of large faults in a given finite mapping area. This typically results in greater downscaling in the throw truncation range than in the fault density range. This causes the data to shift down at the highest throw truncations, the so-called "finite-range effect" [10]. Pickering et al. [10] presents a correction for this effect. The suggested correction was implemented by including the fault density at the two highest throw truncations in the data set for fitting, adding a constant to each fault density in the data set, and calculating a new linear fit. The constant was varied until the square of the correlation coefficient was maximized. A constant of 0.04 mi./mi.^{2} (0.025 km/km^2) provided the best fit. The corrected data and fit are shown on Figure 5b. The C_d resulting from this correction is 1.16.

A comparison of C_d values on Figure 5b provides additional support for taking 1.16 as more accurately representing the fault population. The C_d of 1.43 from the raw data is larger than values typically reported from field studies, which range from 0.5 to 1.0 [5]. Such a value would indicate that the fault network in the Kimberlina area is relatively undeveloped. Additionally, the faults in the vicinity of Kimberlina appear to be primarily growth faults, and so perhaps a lower total strain is reasonable [11]. Conversely, most of the mapped faults intersect other faults, suggesting at least moderate development of the fault network. This would tend to support the contention that a C_d of 1.43 is too large. The corrected C_d of 1.16 shown is more commensurate with the reported range and the observed degree of fault network development. Further, as mentioned, lower values of C_d correlate with a higher density of large offset faults relative to low offset faults. As large offset faults are generally believed to be of more concern for leakage, the lower estimate of C_d is also more conservative with regard to estimating leakage risk.

4.3.Fault encounter probability

As shown in Figure 3, the plume at Kimberlina is anticipated to have an elliptical footprint. Approximating the plume as elliptical, the value of s, the fault-perpendicular plume dimension, can be derived from the plume area, eccentricity and the acute angle between its semi-major axis and the fault orientation of interest. The modeled plume area at Kimberlina, as measured from Figure 3, is 0.83 km^2 (0.32 mi^2). The aspect ratio of the Kimberlina plume from Figure 3 is 1.32. The direction of the plume axis is 60° (updip). The dominant fault strike near Kimberlina, based on the fault orientation analysis, is 170°. Consequently, the acute angle between the semi-major plume axis and the faults is 70°. These values result in s equal to 0.72 km (0.45 mi.).

As a first approximation, the main concern for leakage is for faults with throws that fully offset the sealing formations over the target reservoir. The sealing formation over the storage target in the Vedder has a vertical thickness of approximately 180 m (590 ft). The corrected fault density equation on Figure 5b indicates the average fault density, F, at this throw truncation is 0.028 km/km^2 (0.046 mi./mi.^{2}). This is a low density, so the condition that the fault-perpendicular plume dimension is much smaller than the spacing between faults is sufficiently met to use the probability estimation of Equation 5. Substituting the computed F and s into this equation gives a probability of the numerically-simulated Kimberlina plume encountering a fully seal-offsetting fault of 3.3%.

It is important to note that the numerical model did not incorporate the effect of the fault zones on the bulk phase CO_2 flow, which may in fact control plume shape and direction. As indicated by the corrected power-law distribution in Figure 5b, the density of smaller offset faults is probably quite high. For instance, at a throw truncation of 3 m (10 ft), the density is approximately 3 km/km^2 (5 mi./mi.^{2}). Despite their small offset, the permeability in these fault zones will likely contrast with that of the host rock. Given their high density, it is likely the plume will encounter these small faults and be deflected somewhat to the north. These faults are likely to cause greater elongation of the plume compared to the numerical model results, which were based on isotropic permeability along bedding. A plume aspect ratio of two and an acute angle between the plume axis and the faults of 35° is perhaps more typical due to faulting-induced anisotropy. With these values, the probability of the plume encountering a fully seal-offsetting fault is 2.9% calculated using the approach here.

The plume aspect ratio and the angle between the plume axis and the faults can be treated as variables in the probability estimation method. This affords an understanding of the sensitivity of the probability estimate to variation in these parameters. Figure 6 shows the probability that the Kimberlina plume will encounter a fully seal-offsetting fault across a wide range of plume aspect ratios and the full range of plume axis to fault angles.

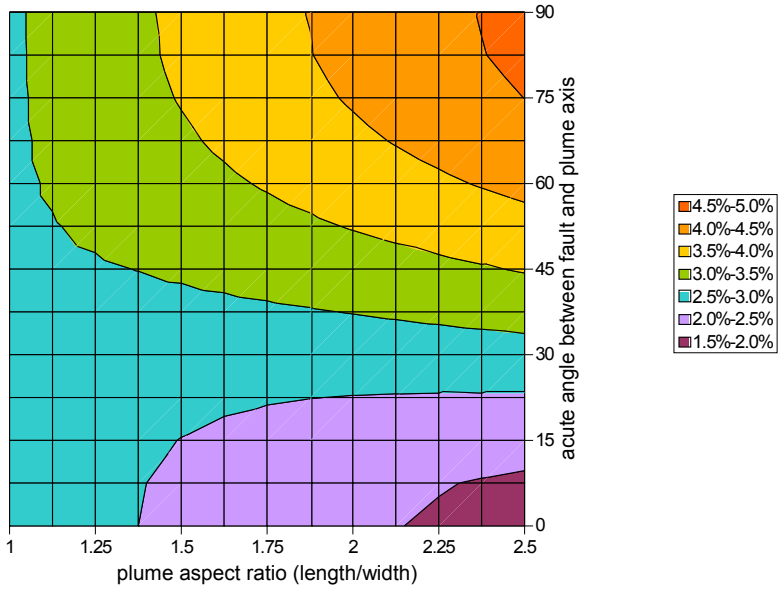

Figure 6. Probability that the Kimberlina plume will encounter a fault fully-offsetting the seal.

The probability of leakage through a fault that fully offsets the seal is considerably less than the probability of the plume encountering such a fault. For instance, shale-gouge ratio (SGR) theory suggests that any point on a fault past which more than 20% of the rock that has slid is shale will tend to have near-shale, rather than near-reservoir-rock permeabilities [12]. By this theory, a fault that just fully offsets a seal consisting of 100% shale will have a minimum SGR of 50% and therefore have low permeability.

5.Conclusions

The goal of the methodology presented in this paper is to estimate the probability that a CO_2 plume will encounter a fault when site-specific data sufficient to allow a deterministic analysis are lacking, but some data from the general area are available. This probability is the first step in estimating the probability of leakage via a fault. As this method is most appropriate before site-specific data are available, its primary applicability is for site screening and early risk assessment. For instance, at some prospective sites, the probability of a plume encountering a fault will be so low as to not warrant the more complicated measurement and/or estimation of fault zone properties. The approach in this paper can provide quantitative information upon which to base such a decision.

This stated, fault population statistics indicate that fault density approaches infinity as the displacement cutoff approaches zero. In practice, most fault population researchers have found, or believe based upon theoretical considerations, that the relationship is accurate down to displacements equivalent to several grain diameters for clastic rocks [3]. Even this implies fault density becomes very large at the actual lower limit of displacement cutoff. This suggests a high probability that a given CO_2 plume will encounter a fault of some size. Of course, most such faults will have such small displacements that they are presumed not be of serious concern in terms of leakage, but this remains to be fully proven.

Acknowledgments

We are grateful to Christine Doughty (LBNL) for sharing the WESTCARB Phase III pilot test simulation results, and to Jeff Wagoner (LLNL) for sharing his expertise regarding the geology of the southern San Joaquin Valley, particularly in the vicinity of the Kimberlina site. This work was supported in part by the CO_2 Capture Project (CCP) of the Joint Industry Program (JIP), and by Lawrence Berkeley National Laboratory under U.S. Department of Energy Contract No. DE-AC02-05CH11231.

References

1. S.M. Benson and P. Cook (coordinating authors), Underground geological storage. In: Intergovernmental Panel on Climate Change Special Report on Carbon Dioxide Capture and Storage, P. Freund (coordinating author). Cambridge University Press, Cambridge, U.K., pp. 195-276, 2005.
2. J. Watterson, J.J. Walsh, P.A. Gillispie and S. Eaton, Scaling systematics of fault sizes on a large-scale range fault map, Journal of Structural Geology, No. 18 (1996) 199 – 214.
3. R.V. Ackerman, R.W. Schlische and M.O. Withjack, The geometric and statistical evolution of normal fault systems: an experimental study of the effects of mechanical layer thickness on scaling laws. Journal of Structural Geology No. 23 (2001) 1803 – 1819.
4. P.A. Cowie, D. Sornette and C. Vanneste, Multifractal scaling properties of a growing fault population, Geophysical Journal International No. 122 (1995) 457 – 469.
5. G. Yielding and R. Fox, Fault population description and prediction using examples from the offshore UK, Journal of Structural Geology No. 18 (1996) 155 – 167.
6. K. Pruess, C.M. Oldenburg, and G. Moridis, TOUGH2 user's guide, version 2.0, Rep. LBNL-43134, Berkeley: Lawrence Berkeley National Laboratory, 1999.
7. K. Pruess and J. García J (2002) Multiphase flow dynamics during CO2 disposal into saline aquifers. Environmental Geology 42: 282-295
8. C. Doughty, Modeling geologic storage of carbon dioxide: comparison of hysteretic and non-hysteretic characteristic curves, Energy Conversion and Management No. 48 (2007) 1768-1781.
9. California Department of Conservation, Division of Oil, Gas and Geothermal Resources, California Oil and Gas Fields, Volume 1, Sacramento, California, 1998.
10. G. Pickering, J.M. Bull and D.J. Anderson, Sampling power-law distributions, Tectonophysics No. 248 (1995) 1-20.
11. B.A. McPherson, Sedimentation and trapping mechanisms in Upper Miocene Stevens and older turbidite fans of the southeastern San Joaquin Valley, California, AAPG Bulletin 62 (1978) 2243 – 2274.
12. G. Yielding, B. Freeman, and D. T. Needham, Quantitative fault seal prediction, AAPG Bulletin No. 81 (1997) 897 – 917.